Accuracy Optimization and Wide Limit Constraints of DC Energy Measurement Based on Improved EEMD

Xiaoyu Wang*, Xin Yin, Xinggang Li, Jiangxue Man, Yanhe Liang, Fan Xu
State Grid Heilongjiang Electric Power Co. Ltd. Marketing Service Center; Power Metering Center, Harbin, 150000, China

***Abstract*—In modern power systems, with the increasing application of renewable energy, direct current transmission technology has put forward new requirements for energy metering. In order to solve the accuracy problem of traditional electric energy metering under DC energy, the research is based on the classical empirical modal decomposition (EEMD), and introduces the artificial chemical reaction optimization algorithm (ACROA) to enhance the global search capability and decomposition accuracy of the original algorithm, and at the same time safeguards the accuracy of metering equipment under extreme conditions through the wide quantitative constraints, and ultimately puts forward a new type of optimization model for the accuracy of DC electric energy metering. The highest measurement accuracy of this model could reach 90%, and it performed better in power signal decomposition and accuracy optimization. Especially under high-frequency interference and complex signal conditions, the measurement error could be reduced to 6.87%, the highest decomposition stability was 94.02%, and the shortest measurement time was 1.12 seconds. Therefore, the model constructed in this study exhibits excellent decomposition accuracy and robustness in complex energy environments, solving the shortcomings of traditional energy metering methods and providing new ideas for future optimization of DC energy metering.**

***Keywords*—EEMD; direct current energy; measurement; width limit; ACROA**

I. Introduction

In modern power systems, with the transformation of energy structure, Direct Current (DC) transmission technology has been increasingly widely used, especially in renewable energy generation such as wind power, photovoltaic power generation, and electric vehicle charging piles, where the demand for direct current energy is gradually increasing [1]. This trend has put forward new requirements for Direct Current Energy Metering (DCEM) technology. Existing power metering equipment is mainly designed for AC power grids, with low metering accuracy and stability in DC environments, making it difficult to cope with complex signal conditions and extreme operating conditions, such as significant increase in metering error under high voltage and high current, and insufficient decomposition capability when disturbed by noise and non-stationary signals [2]. Therefore, there is an urgent need to explore optimization methods that can maintain high-precision metering in complex DC energy environments. The study aims to solve the core problem in DC energy metering, which is how to ensure the accuracy, stability and adaptability of metering equipment under complex working conditions and extreme conditions. To this end, the study proposes a metering accuracy optimization model that combines the improved EEMD with the artificial chemical reaction optimization algorithm, and further improves the adaptability and reliability of the model in different voltage and current ranges by introducing a wide-volume-limit constraint. The objective of the research is to improve the decomposition accuracy and robustness of DC energy signals, and to significantly reduce the metering error and computation time by improving the signal decomposition and optimization algorithm. The importance and significance of the study is to break through the limitations of the traditional DC energy metering methods, to provide an efficient, stable and adaptable metering technology for DC transmission and renewable energy, to provide new ideas for the optimization of power metering under complex working conditions in future smart grids, and to provide important theoretical and practical references for the researchers in the related fields to explore the signal processing methods based on EEMD.

II. Related Work

For power metering in DC environment, many researchers at home and abroad have successively explored the technology and proposed many accuracy optimization methods. Buchibabu et al. proposed a comprehensive control strategy to better manage the storage of DC microgrids such as AC power grids, by combining tuna swarm optimization algorithms, which could effectively improve the level of various DCEMs in microgrids [3]. Gao J et al. proposed an energy compensation algorithm limited to DC microgrids using intelligent optimization algorithms, whose error was also smaller than the traditional average EM algorithm, and the real-time power curve was closer to the theoretical value [4]. To further improve the accuracy of DCEM, Liaqat R et al. constructed a signal decomposition model using event matching energy decomposition algorithm after receiving non-invasive load monitoring, which could effectively distinguish various types of noise in electrical energy, thereby improving computational accuracy [5]. Kumar G et al. used optimized tracking algorithms to process data on appliance usage frequency, preferred operating interval, and average power consumption to better calculate household energy consumption within microgrids. This method could significantly improve the accuracy of electricity calculation and reduce time costs. But at this time, the usage cost and computational complexity actually increased, which had an impact on the overall calculation [6].

However, most of these methods are optimized for specific scenarios, which makes it difficult to maintain high accuracy under complex or extreme electrical energy signals, and they are deficient in high-frequency noise processing and real-time optimization. In addition, currently, Empirical Mode Decomposition (EMD) and its improved algorithms, such as Ensemble Empirical Mode Decomposition (EEMD), have gradually attracted the attention of researchers due to their unique advantages in signal decomposition [7]. Liang C et al. proposed a control strategy combining EEMD to improve the power time series regulation accuracy of DC microgrid photovoltaic power generation and its hybrid energy storage system, which could achieve better control effects under different power fluctuation characteristics [8]. Jiang L et al. proposed a wavefront calibration method to accurately locate the fault location in DC distribution systems by combining EEMD and singular value decomposition algorithms. This method could accurately decompose DC power signals and had high accuracy in fault location [9]. Zhang N et al. proposed a novel accuracy prediction model for short-term photovoltaic power generation by combining EEMD and gated recursive units. The prediction accuracy and robustness of this model are superior [10]. Wang et al. proposed a novel fault localization strategy by combining EEMD and adaptive local mean decomposition methods. This method detected DC series arc faults in less than 1ms with an accuracy of 98.75% [11].

In summary, previous studies have made many useful explorations in improving the accuracy of DC energy metering and processing complex signals. However, these researches still have some shortcomings when facing extreme working conditions, such as high voltage and high current, for example, the accuracy degradation during signal decomposition and low arithmetic efficiency. For this reason, how to develop a DC energy metering method that is efficient, robust and applicable to complex working conditions has become a key issue to be solved. The research focuses on solving the lack of metering accuracy of traditional methods, and by improving the EEMD algorithm and introducing the Artificial Chemical Reaction Optimization Algorithm (ACROA), a new type of DC energy metering model is proposed, and at the same time, the metering equipment is enhanced by the wide quantitative constraints under extreme working conditions, such as high voltage and high current. The research objectives include improving the decomposition accuracy of complex signals, reducing the metering error, optimizing the real-time performance of the model, and enhancing the stability of the model under the wide quantitative constraints. The importance of this study is that it makes up for the shortcomings of the existing methods and provides theoretical support and technical guarantee for the DC transmission system in the future smart grid and energy internet, which is of great theoretical and engineering significance.

III. Methods and Materials

A. DC Signal Decomposition

Due to the complexity of DC electrical signals, traditional measurement methods are difficult to cope with non-stationary, nonlinear, and the superposition of various interference signals [12]. There are many factors that affect the error of EM, and to minimize the error in DCEM, the primary requirement is to ensure the stability of the data acquisition source. DC energy meters are core devices used to measure DC, voltage, and related electrical parameters [13]. It can directly complete DCEM independently, and Fig. 1 shows the working principle of a DC energy meter.

In Fig. 1, firstly, the current sampling and voltage sampling modules collect the load current I and load voltage U. The collected current signal is used for power calculation with the voltage signal through a multiplier, and then converted into a frequency signal through a power frequency converter. Next, the frequency divider processes the frequency signal for subsequent calculation and display. The signal processing unit calculates based on the divided data and transmits the final electrical energy information to the counting display module. In this process, the main challenges of DCEM are as follows: traditional measurement methods are difficult to effectively handle these complex signals; The range of the measuring device is limited, and when extreme conditions are encountered, the measuring equipment often experiences over range problems, leading to increased measurement errors; DCEM equipment is susceptible to environmental interference during long-term operation, leading to fluctuations in measurement results [14-15]. Taking into account the above factors, this study assumes the existence of an ideal DCEM. Fig. 2 shows the classification of DC electrical signals at this time.

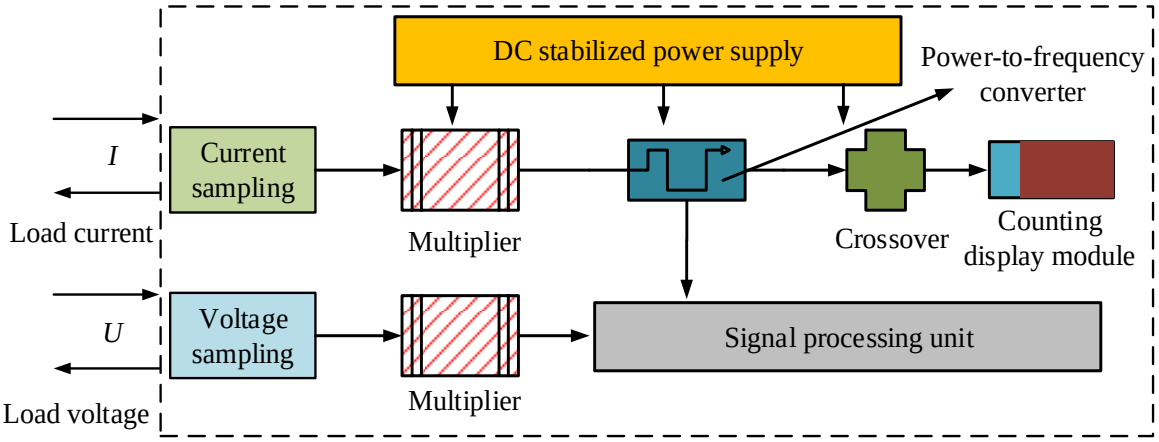

Fig. 1. DC energy meter working principle diagram.

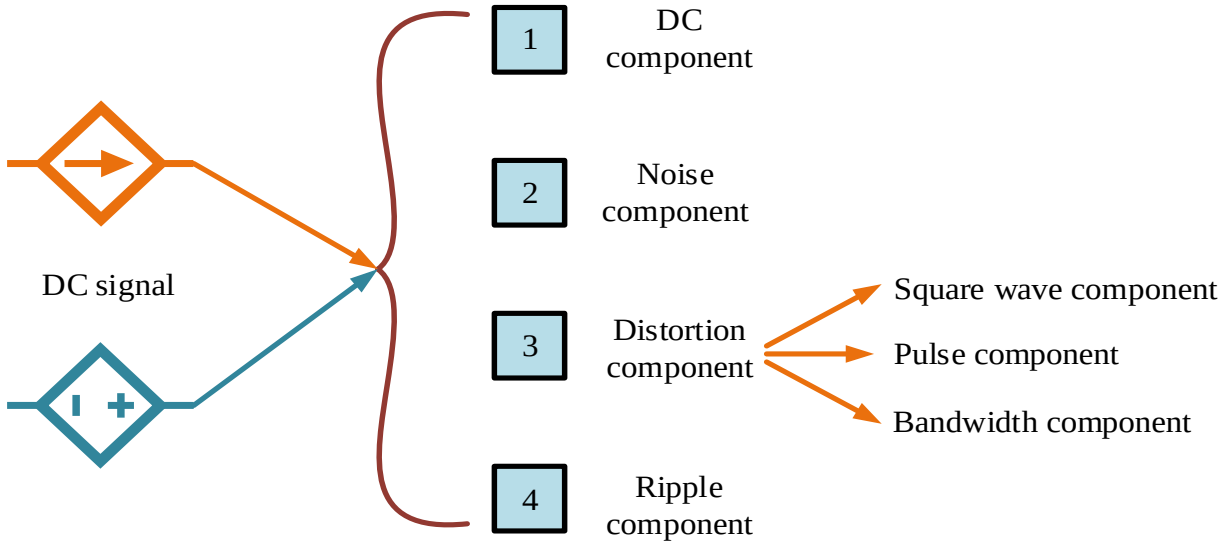

Fig. 2. DC signal composition classification.

In Fig. 2, DC electrical signals are DC components, noise components, distortion components, and ripple components. The DC component represents the stable part of the signal and is the main carrier of energy transmission; the noise component is mainly generated by random interference brought by external environment or equipment, which may include the influence of external factors such as temperature and humidity [16]. The expression of the DC electrical signal at this time is shown in Eq. (1).

$$u(t) = u_0 + \sum_n u_n(t) + \sum_i u_i(t) + \sum_k u_k(t) \quad (1)$$

In Eq. (1), $u(t)$ represents the DC electrical signal; $\sum_n u_n(t)$ represents the noise component; $\sum_i u_n(t)$ represents the distortion component; $\sum_k u_k(t)$ represents the ripple component. The ideal expression of the DC component is shown in Eq. (2).

$$u_1(t) = k(t) \quad (2)$$

In Eq. (2), k represents a constant; $u_1(t)$ represents the DC component in the ideal state. The noise component in the ideal state is usually avoided by adding noise compensation or filtering devices. At this time, the white noise signal with a specific noise ratio is composed as shown in Eq. (3).

$$u_2(t) = n(t) \quad (3)$$

In Eq. (3), n represents the white noise signal in the noise ratio; $u_2(t)$ represents the noise component in the ideal state. The distortion component originates from the use of nonlinear loads, causing signal deformation. For example, the fluctuating charge and discharge signals generated when the load is involved or the power grid system is disconnected [17]. Common distortion signals such as square wave components and broadband components are expressed in Eq. (4).

$$\begin{cases} u_3(t) = u_1(t) \pm A \times k_1(t) & 0 \le t \le t_1 \\ u_4(t) = u_1(t) - B(t - t_2)^2 + b_1(t) & t_1 \le t \le t_2 \end{cases} \quad (4)$$

In Eq. (4), A represents the amplitude multiple of the signal component; t represents time, where t_1 and t_2 represent the start and end times, respectively; k_1 represents the time period t_1 to t_2 control constant. The ripple component reflects the periodic interference caused by power supply ripple, which is usually characterized by high-frequency and small amplitude periodic fluctuations. The expression of the ripple component is shown in Eq. (5).

$$u_5(t) = D \times u_1(t) \times \sum_{t=1}^{n} \cos(2\pi i \omega_1 t), 0 < D < 0.1 \quad (5)$$

In Eq. (5), ω_1 represents a constant; ω_1 represents frequency. However, in the process of decomposing DC electrical signals, due to the discontinuity and complexity of the signal, Gibbs phenomenon is prone to occur, that is, oscillation occurs at the high-frequency components or abrupt points of the signal, resulting in overshoot or fluctuation during signal reconstruction, which affects the accuracy of measurement [18]. This phenomenon is particularly evident when dealing with non-stationary and nonlinear signals. Fig. 3 is a typical schematic diagram of Gibbs phenomenon.

Both Fig. 3 (a) and Fig. 3 (b) show the time-domain waveform of Gibbs phenomenon. In Fig. 3, after Fourier series expansion of periodic functions with discontinuous points, finite terms are selected for synthesis. As the number of selected items increases, the peak in the synthesized waveform gradually approaches the discontinuity point of the original signal. When the number of terms is sufficient, the peak tends towards a constant, approximately 9% of the total jump variable.

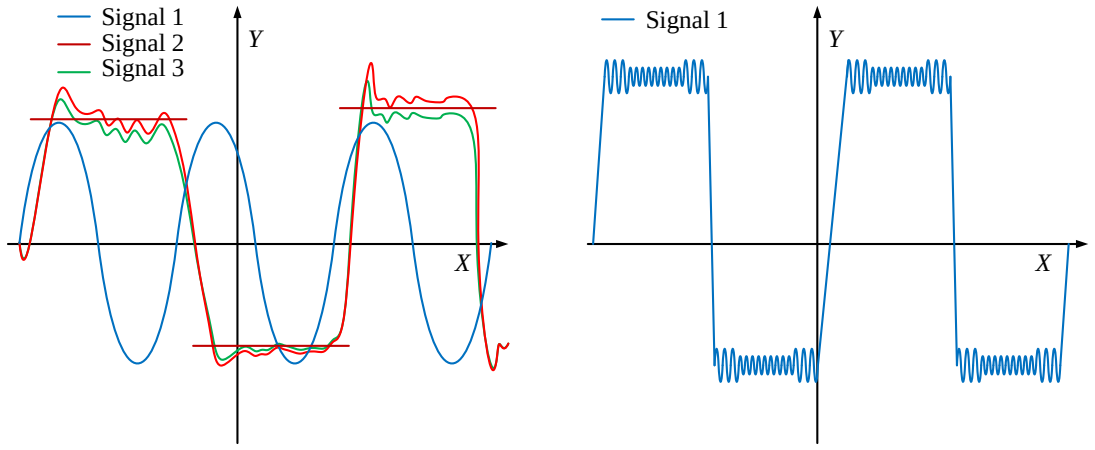

(a) The Gibbs phenomenon1 (b) The Gibbs phenomenon2

Fig. 3. Example of the Gibbs phenomenon.

B. DCEM Accuracy Optimization and WLC Based on Improved EEMD

To overcome the Gibbs phenomenon, EEMD is introduced in this study. EEMD can effectively reduce the influence of Gibbs phenomenon in signal decomposition, improve the accuracy of signal reconstruction, and exhibit better robustness and stability in various complex signal environments [19]. Fig. 4 shows the process of EEMD.

In Fig. 4, firstly, white noise of different intensities is added to the original signal and stacked multiple times. Next, each superimposed signal is subjected to empirical mode decomposition to obtain a series of Intrinsic Mode Functions (IMF). Then, all IMF components are averaged to eliminate uncertainty introduced by noise. However, as a signal decomposition method with non Fourier transform, EEMD may still face the problem of insufficient decomposition accuracy when dealing with specific complex signals. Therefore, ACROA is introduced in this study to further optimize the decomposition process. ACROA first generates a set of reactants through initialization. Secondly, in the subsequent iteration process, different chemical reaction operators are dynamically selected and operated based on the current signal state and optimization requirements to adapt to different signal conditions [20]. Then, after each reaction, the reactants are updated based on feedback, similar to a reversible reaction process. This process involves redox reactions, decomposition reactions, displacement reactions, and synthesis reactions. Fig. 5 shows an example of the reaction.

In Fig. 5 (a), the redox reaction mechanism optimizes the global search capability of the signal by adjusting the state of the reactants to change their energy levels; In Fig. 5 (b), the decomposition reaction decomposes complex signals into smaller units, thereby improving the local search accuracy of the algorithm; In Fig. 5 (c), the substitution reaction enables the algorithm to quickly jump out of local optima and improve global search efficiency through the exchange of reactants; In Fig. 5 (d), the synthesis reaction helps the algorithm find a better solution by combining multiple signal components. At this point, the optimized DC power signal decomposition is shown in Eq. (6).

$$X(t) = \sum_{i=1}^{n} IMF_i(t) + r_n(t) \tag{6}$$

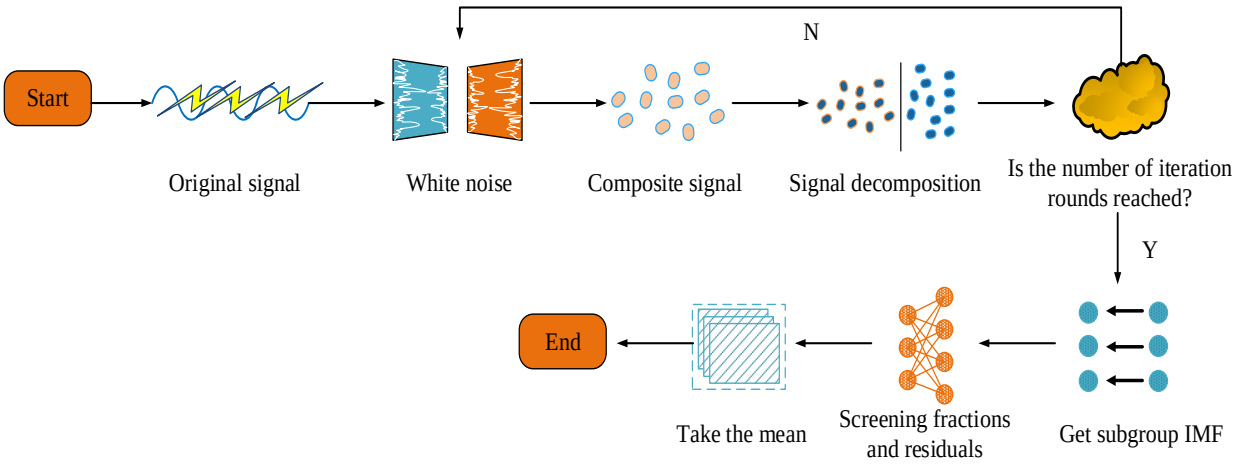

Fig. 4. EEMD process schematic.

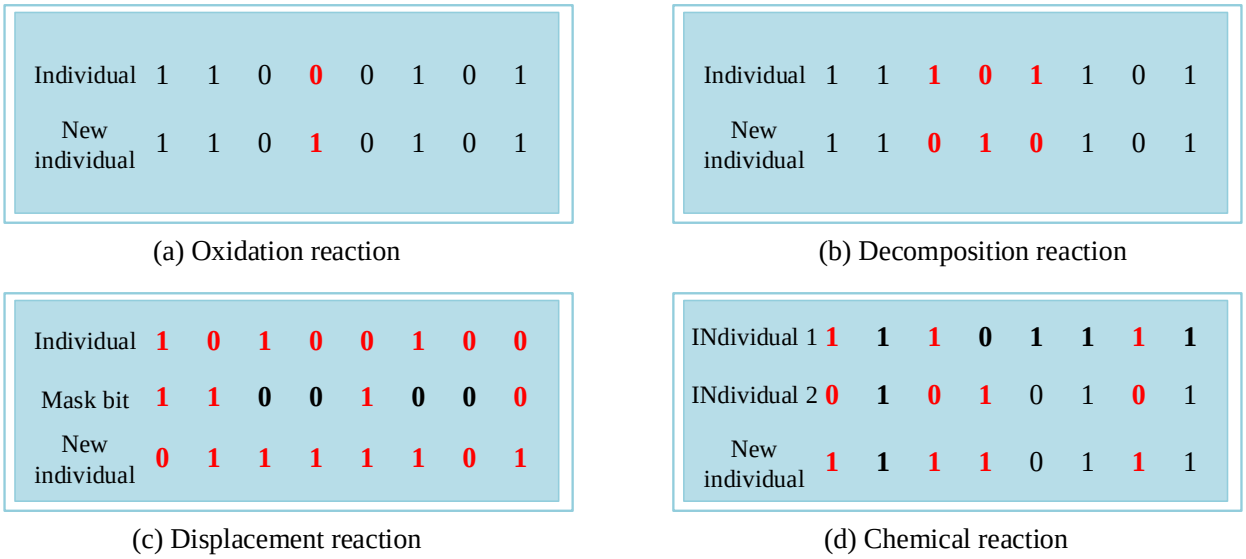

Fig. 5. Schematic of ACROA's four binary coded responses.

In Eq. (6), $X(t)$ represents the original DC electrical signal; $X(t)$ represents the -i th eigenmode function; $r_n(t)$ represents the residual term, which is the remaining part after signal decomposition; n represents the number of decomposed eigenmode functions. After obtaining these IMF components through the EEMD algorithm, ACROA is used to further optimize the accuracy of the residual term $r_n(t)$ to reduce decomposition errors. The calculation equation is shown in Eq. (7).

$$r_{opt}(t) = \min_{\alpha}(r_n(t) - \alpha\Delta r(t)) \tag{7}$$

In Eq. (7), $r_{opt}(t)$ represents the residual term after optimization; α represents the optimal weight coefficient obtained during the ACROA optimization process; α represents the adjustment amount during the ACROA iteration process, which is the correction value obtained through the reaction mechanism optimization in each iteration. The combination of the two results in the final optimization signal $X_{opt}(t)$ calculation equation is shown in Eq. (8).

$$X_{opt}(t) = \sum_{i=1}^{n} IMF_i(t) + r_{opt}(t) \tag{8}$$

In addition, each frequency component in the signal may have different characteristics within different limits. To ensure the stability and reliability of the energy meter in the face of extreme conditions, this study has imposed constraints on the Wide Dynamic Range (WDR). Among them, WDR refers to a large range that can be accurately measured or processed in measuring or measuring equipment, that is, the equipment can maintain high accuracy and reliability over a wide range of input signal amplitudes. For DCEM, WDR usually means that the measuring equipment can maintain measurement accuracy without significant errors over a wide range of changes from low voltage and low current to high voltage and high current. The WDR constraint is shown in Eq. (9).

$$L_{\min} \le X_{opt}(t) \le L_{\max} \tag{9}$$

In Eq. (9), $L_{\min}$ and $L_{\max}$ represent the upper and lower limits of the measured DC signal, respectively. The constraint error calculation equation at this time is shown in Eq. (10).

$$\varepsilon(t) = \left| X(t) - X_{opt}(t) \right| \le \delta \tag{10}$$

In Eq. (10), $\varepsilon(t)$ represents the error between the measured signal and the optimized signal; $X(t)$ represents the actual measured DC signal; δ represents the maximum allowable error limit. To adapt to the dynamic changes in the measurement environment and ensure that the signal can be adaptively adjusted under WDR, the dynamic range expression of WDR at this time is shown in Eq. (11).

$$X_{opt}(t) = \max(\frac{X(t)}{L_{\max}}), and \min(\frac{X(t)}{L_{\min}}) \tag{11}$$

This study combines EEMD-ACROA and WDR to propose a novel DCEM model. Fig. 6 shows the process of the model.

In Fig. 6, the DC electrical signal is first collected and preprocessed through current and voltage sampling modules to ensure signal stability. Then, the DC electrical signal decomposition model is constructed, and the signal is divided into DC components, noise components, distortion components, and ripple components to reflect the main characteristics of the signal. Then, the EEMD algorithm is used to decompose the signal, obtain the intrinsic mode functions of different frequencies, and optimize the residual terms through the ACROA algorithm to dynamically adjust the reaction path and reduce decomposition errors. WLC is introduced to ensure that equipment maintains high-precision measurement under extreme conditions such as high voltage and high current. The signal processing process is optimized through an error control mechanism, and the optimized electrical energy data is transmitted to the display module for real-time monitoring and accurate measurement.

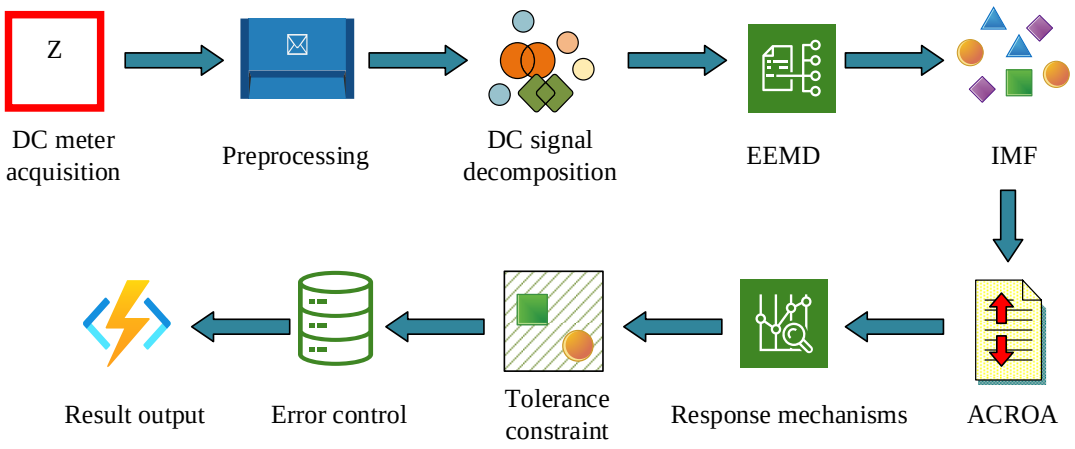

Fig. 6. Novel DCEM modeling process.

IV. Result

A. Performance Testing of the New DCEM Model

The experimental hardware was Keysight E36312ADC power supply, with an output range of 0-100V and a maximum current of 10A. The load simulator was Chroma 63206A-150-600, which supported a maximum of 600W. The precision current sensor was LEM HAZ 1000-S, with a current range of 0-1000A and an accuracy of ±0.1%. The data was collected through the National Instruments NI USB-6343 high-precision data acquisition card. The software part was Dell Precision 5820 Tower, equipped with Intel Core i9-10900X processor, 64GB DDR4 memory, 2TB SSD hard drive, and NVIDIA Quadro RTX 4000 GPU. Python 3.10 was used for data analysis and visualization. The IEEE PES Distribution Test Feeder Dataset (IEEE PES) and Electric Power Consumption Dataset (EPC) datasets were the sources of test data. IEEE PES included various typical electrical energy signals in distribution systems, especially voltage and current waveform data for different loads and grid conditions; EPC contained a series of energy consumption data for household users, including current, voltage, power, and other related information. This study first conducted ablation testing on the proposed algorithm model. Fig. 7 shows the test results.

In Fig. 7 (a), after 200 iterations, the measurement accuracy of EEMD-ACROA-WDR continued to remain at a high level and reaches nearly 90% accuracy at 600 iterations. It performed even better in terms of global optimization capability and robustness. In Fig. 7 (b), EEMD-ACROA-WDR achieved a measurement accuracy of over 90% after 300 iterations. Although EEMD-ACROA performed well in the early iterations, there were significant fluctuations in the later stages, and the measurement accuracy did not steadily improve. Overall, the modules of EEMD-ACROA-WDR demonstrated stronger adaptability and stability on both datasets. The study introduced advanced DCEM precision optimization methods for comparison, namely Bispectral Analysis (BA), Extreme Learning Machine (ELM), and Adaptive Local Mean Decomposition (ALMD). The signal decomposition rate was used as the indicator to test the power processing capability under different bandwidth ranges, as shown in Fig. 8.

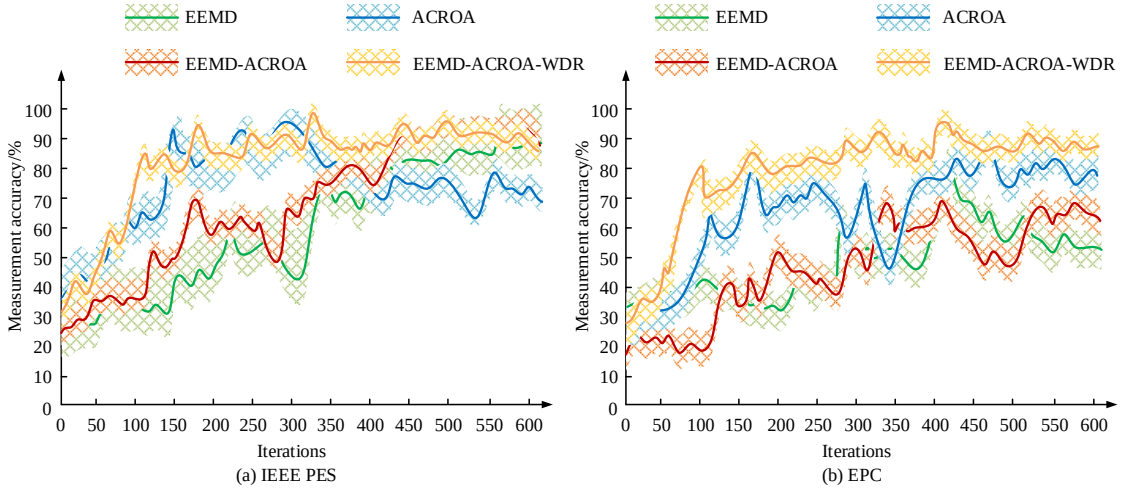

Fig. 7. Ablation test results.

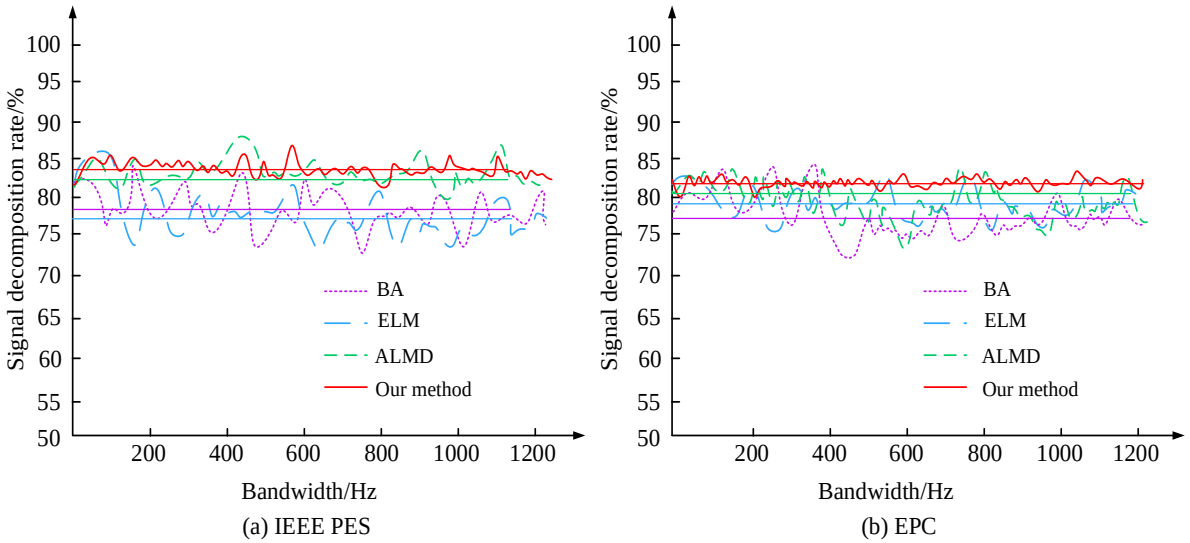

Fig. 8. Signal decomposition rate test results of different methods.

In Fig. 8, within different bandwidth ranges, the proposed method maintained a signal decomposition rate of around 85% with minimal fluctuations at higher bandwidths, such as 800Hz to 1200Hz, demonstrating good stability. The decomposition rates of BA and ELM showed significant fluctuations at high bandwidth, especially the decomposition rate of BA method was relatively unstable throughout the entire bandwidth range, with an average decomposition rate of only 78%. Overall, the proposed optimization algorithm exhibited stronger adaptability and decomposition ability in processing high bandwidth signals, especially maintaining high signal decomposition rates on IEEE PES and EPC, verifying the effectiveness of the algorithm in complex signal environments. In Table I, the precision, recall, F1 value, and average time for precision optimization in DCEM were used as indicators for this study.

TABLE I. INDICATOR TEST RESULTS FOR EACH METHOD

Data Set	Method	P/%	R/%	F1/%	Average Time Spent/S
IEEE PES	BA	87.63	84.12	85.88	2.11
	ELM	84.25	85.36	84.81	2.03
	ALMD	89.74	87.15	88.45	1.54
	Our method	90.11	89.63	89.87	1.02
EPC	BA	88.53	85.16	86.85	2.12
	ELM	89.68	86.84	88.26	1.76
	ALMD	90.08	88.45	89.27	1.52
	Our method	90.87	89.74	90.31	1.08

In Table I, on IEEE PES, the proposed method had the highest P-value of 90.11%, R-value of 89.63%, and F1 value of 89.87%, all of which were higher than other methods, indicating its higher accuracy and stability in signal processing and EM aspects. Meanwhile, the average time was 1.02 seconds, which was much lower than other methods, reflecting the efficiency advantage of this algorithm. In contrast, although ALMD performs better in accuracy and F1 score, it took 1.54 seconds and had a relatively slower processing speed. BA and ELM were slightly lower than the proposed method in various indicators, especially in terms of time. BA took 2.11 seconds, which was more time-consuming. For EPC, the proposed method achieved a P-value of 90.87%, an R-value of 89.74%, and an F1 value of 90.31%, demonstrating excellent performance with a time of 1.08 seconds and a significant advantage in speed.

B. New DCEM Model Simulation Testing

This study set the amplitude of the original current signal to 2A and simulated the input of electrical energy signals under different operating conditions. The simple EEMD model and the proposed method were compared and tested for signal decomposition to evaluate the robustness and decomposition accuracy of different models in processing complex DC signals, as shown in Fig. 9.

In Fig. 9 (b) - Fig. 9 (d), the decomposed electric energy signals IMF1, IMF2, and IMF3 of the EEMD model exhibited significant oscillations and noise, especially in IMF1 and IMF3, where multiple irregular pulse points appear, which had a negative impact on the stationarity and decomposition accuracy of the signal. This indicated that EEMD still faced certain noise aliasing problems when processing complex electric energy signals. The proposed method decomposed IMF1, IMF2, and IMF3 to be smoother, with significantly reduced oscillation amplitude, indicating that this method had better performance in noise suppression and signal smoothing. Especially in the decomposition of IMF3, the proposed method effectively eliminated high-frequency noise and irregular fluctuations in the original signal, preserving the main features of the signal. This indicated that the proposed method could better capture the true characteristics of signals when dealing with non-stationary signals and high-frequency interference, improving the accuracy and stability of DCEM. In Fig. 10, this study conducted signal accuracy tests on EEMD before and after improvement.

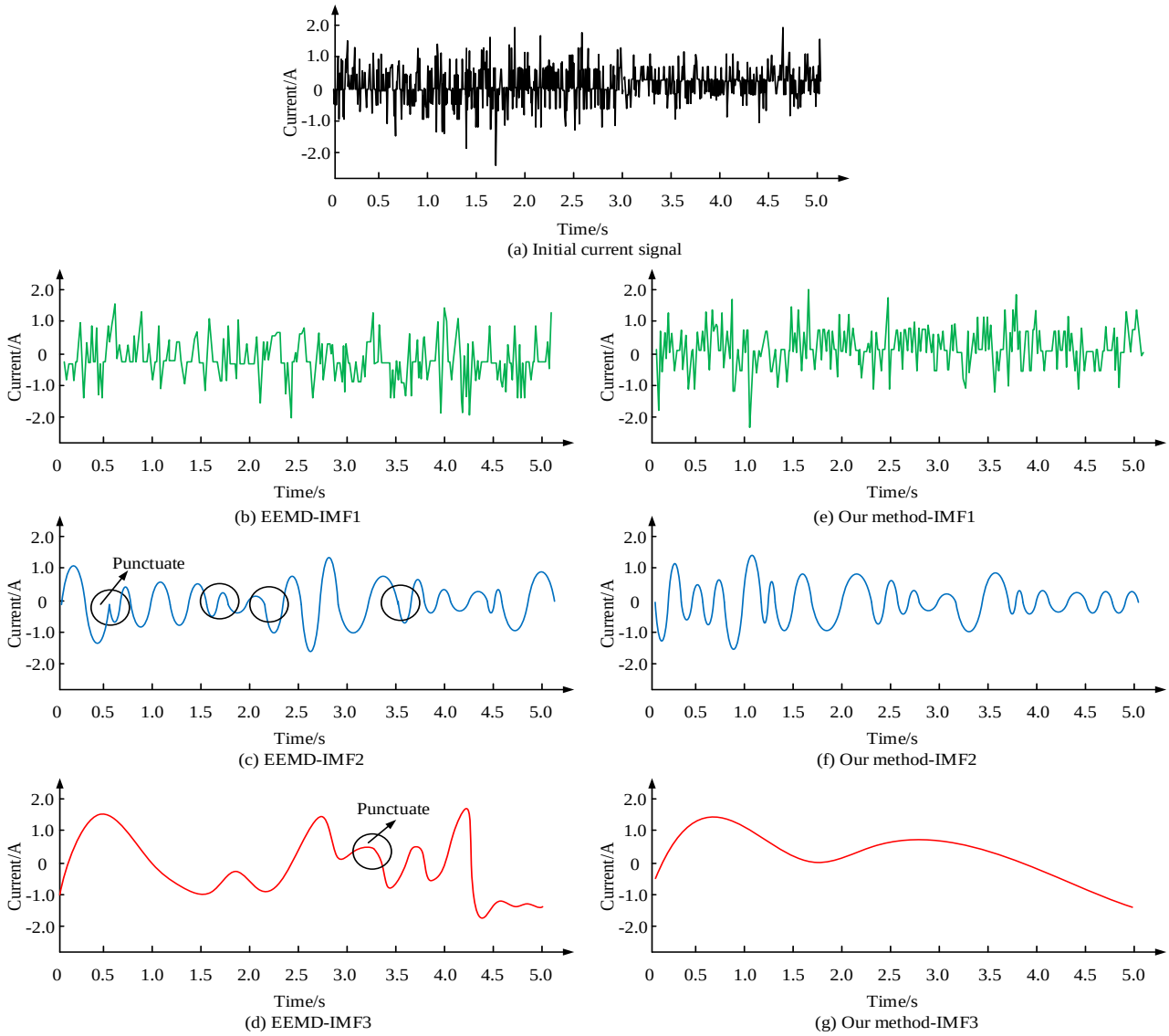

Fig. 9. Decomposition testing of electrical energy signals for two types of models.

In Fig. 10 (a) -10 (c), the measured values of EEMD in the IMF1 signal deviate significantly from the true values and fluctuated greatly, indicating that EEMD had insufficient accuracy in processing high-frequency signals. In the IMF2 and IMF3 signals, although the matching between the measured values and the standard values improved, there were still significant errors, especially at certain peak points, indicating that the EEMD method also had certain errors in processing low-frequency signals. In Fig. 10 (d) -10 (f), the measured values almost completely coincided with the standard values in the IMF2 and IMF3 signals, indicating that the proposed method outperformed traditional EEMD in processing low-frequency signals. Meanwhile, the error of IMF1 signal was effectively controlled, demonstrating better signal reconstruction capability. Overall, the proposed method performed better in terms of measurement accuracy and stability, especially when dealing with complex signals, with significantly reduced errors, verifying the practical application effect of the model in EM. In Table II, this study tested the number of IMF decompositions, measurement error, decomposition stability, and computation time as indicators.

In Table II, in terms of the number of IMF decompositions, the proposed method was the same as methods such as BA and ALMD, both of which decomposed into 6 IMF components, indicating its high decomposition ability in processing complex electrical energy signals. In terms of measurement error, the proposed method had an error of 6.87%, significantly lower than other methods, indicating higher accuracy in EM and stronger robustness, especially when dealing with noise and non-stationary signals. In terms of decomposition stability, the proposed method had a decomposition stability of up to 94.02%, which was better than the 92.48% of Wang L et al.'s method, demonstrating stability and consistency in signal decomposition, greatly reducing error fluctuations. In terms of computation time, the proposed method took 1.12 seconds, which was the fastest among all methods, far lower than the BA method's 2.34 seconds, demonstrating its high efficiency in practical applications.

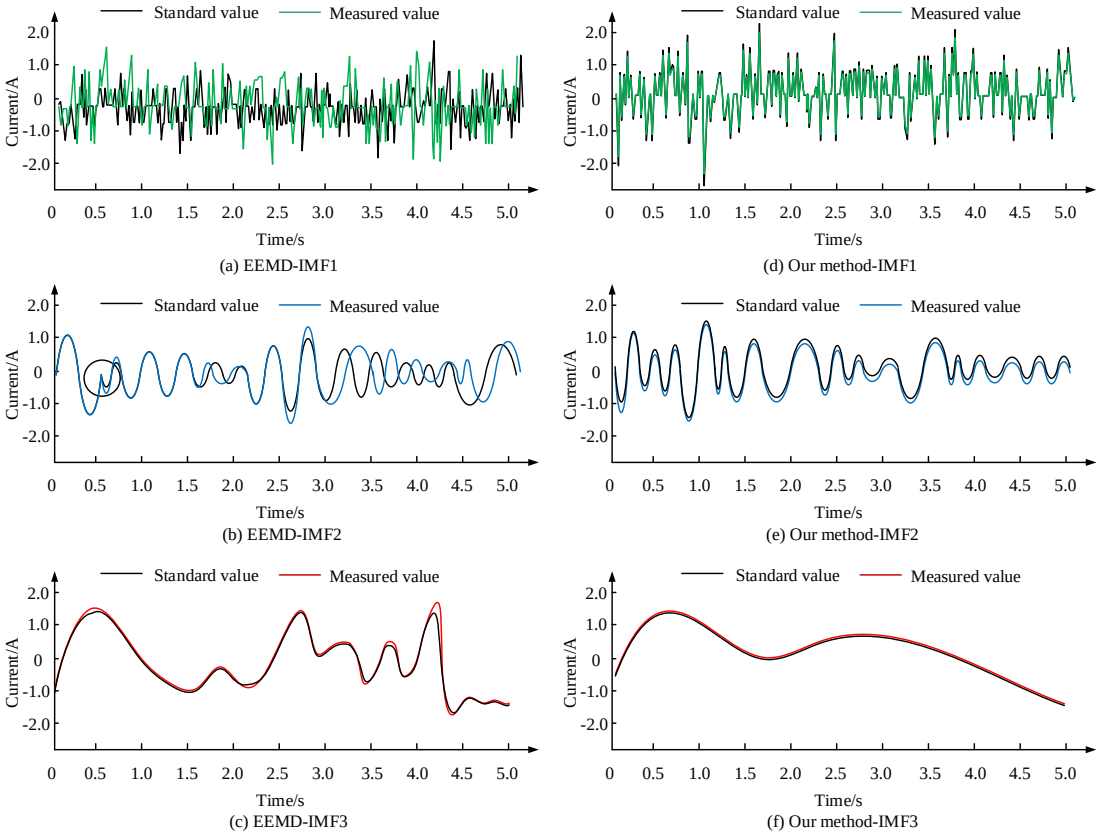

Fig. 10. Results of the comparison of the measurement errors of the two types of methods.

TABLE II. MULTI-INDICATOR TEST RESULTS FOR DIFFERENT MEASUREMENT METHODS

Method	Number of IMF Decompositions	Measurement Error/%	Decomposition Stability/%/%	Operation Time/S
BA	6	12.34	85.56	2.34
ELM	5	10.89	87.12	1.89
ALMD	6	9.78	88.34	1.52
EEMD	7	11.56	86.47	1.74
The method proposed by Liang C et al.	6	8.98	89.65	1.62
The method proposed by Jiang L et al.	5	8.45	90.12	1.58
The method proposed by Zhang N et al.	7	7.89	91.05	1.43
The method proposed by Wang L et al.	6	7.34	92.48	1.32
Our method	6	6.87	94.02	1.12

V. CONCLUSION

In response to the problems of low accuracy of DCEM and insufficient robustness of traditional methods in complex electrical signals, this study proposes a DCEM accuracy optimization method that combines improved EEMD and ACROA, and improves the adaptability of measuring equipment in extreme working conditions by introducing WLC. The proposed model could achieve an accuracy of nearly 90% in the lowest 300 iterations. Compared with the BA, ELM, and ALMD models, the signal decomposition rate of the proposed model was significantly better than other methods, especially under higher bandwidth conditions such as 800Hz to 1200Hz. Its signal decomposition rate was as high as nearly 85%, with the highest P value of 90.87%, the highest R value of 89.74%, and the highest F1 value of 90.31%. The average optimization time for accuracy was as short as 1.02 seconds. The proposed model decomposed IMF1, IMF2, and IMF3 to be smoother, with significantly reduced oscillation amplitude, indicating better performance in noise suppression and signal smoothing. Meanwhile, the proposed model significantly reduced the error between the measured values of the three types of IMF signals and the true values, and had better processing accuracy than traditional EEMD. The maximum number of IMF components was 6, the lowest measurement error was 6.87%, the highest decomposition stability was 94.02%, and the shortest measurement time was 1.12 seconds. In summary, the proposed model has advantages in efficiency in practical applications.

However, the model has not carried out an in-depth study on the impact of external factors such as changes in environmental temperature and humidity on the metering accuracy. Future research can consider introducing an environmental adaptive mechanism, monitoring environmental changes in real time through temperature and humidity sensors, and dynamically adjusting the metering model by combining with adaptive algorithms. In addition, the expansion of the model can include improving the processing capability of ultra-high frequency noise signals, optimizing the model parameters to further reduce the computation time, as well as combining with the Internet of Things and big data analysis technology to achieve multi-device collaborative metering, and constructing a more comprehensive power monitoring system. These improvements will help to further enhance the practicality and adaptability of the model to meet the needs of more complex and diverse application scenarios.

REFERENCES

[1] Chen Z, Amani A M, Yu X, Jalili M. Control and optimisation of power grids using smart meter data: A review. Sensors, 2023, 23(4): 2118-2124.

[2] Rind Y M, Raza M H, Zubair M, Mehmood M Q, Massoud Y. Smart energy meters for smart grids, an internet of things perspective. Energies, 2023, 16(4): 1974-1981.

[3] Buchibabu P, Somlal J. Green energy management in DC microgrids enhanced with robust model predictive control and muddled tuna swarm MPPT. Electrical Engineering, 2024, 106(3): 2799-2819.

[4] Gao J, Wang X, Yang W. SPSO-DBN based compensation algorithm for lackness of electric energy metering in micro-grid. Alexandria Engineering Journal, 2022, 61(6): 4585-4594.

[5] Liaqat R, Sajjad I A. An event matching energy disaggregation algorithm using smart meter data. Electronics, 2022, 11(21): 3596-3597.

[6] Kumar G, Kumar L, Kumar S. Multi-objective control-based home energy management system with smart energy meter. Electrical Engineering, 2023, 105(4): 2095-2105.

[7] Chou S Y, Dewabharata A, Zulvia F E. Forecasting building energy consumption using ensemble empirical mode decomposition, wavelet transformation, and long short-term memory algorithms. Energies, 2022, 15(3): 1035-1037.

[8] Liang C, Ren W, Cheng P. Control strategy of photovoltaic DC microgrid based on fuzzy EEMD. Tehnički vjesnik, 2022, 29(5): 1762-1769.

[9] Jiang L, Xia L, Zhao T, Zhou J. An improved arc fault location method of DC distribution system based on EMD-SVD decomposition. Applied Sciences, 2023, 13(16): 9132-9133.

[10] Zhang N, Ren Q, Liu G, Guo L, Li J. Short-term PV output power forecasting based on CEEMDAN-AE-GRU. Journal of Electrical Engineering & Technology, 2022, 17(2): 1183-1194.

[11] Wang L, Lodhi E, Yang P, Qiu H, Rehman W U, Lodhi Z, Tamir T S, Khan M A. Adaptive local mean decomposition and multiscale-fuzzy entropy-based algorithms for the detection of DC series arc faults in PV systems. Energies, 2022, 15(10): 3608-3611.

[12] Laayati O, Bouzi M, Chebak A. Smart energy management system: design of a monitoring and peak load forecasting system for an experimental open-pit mine. Applied System Innovation, 2022, 5(1): 18-21.

[13] Ding T, Jia W, Shahidehpour M. Review of optimization methods for energy hub planning, operation, trading, and control. IEEE Transactions on Sustainable Energy, 2022, 13(3): 1802-1818.

[14] Thirugnanam K, El Moursi M S, Khadkikar V, Zeineldin H H, Hosani M A. Energy management strategy of a reconfigurable grid-tied hybrid AC/DC microgrid for commercial building applications. IEEE Transactions on Smart Grid, 2022, 13(3): 1720-1738.

[15] Bhattar C L, Chaudhari M A. Centralized energy management scheme for grid connected DC microgrid. IEEE Systems Journal, 2023, 17(3): 3741-3751.

[16] Badr M M, Ibrahem M I, Kholidy H A, Fouda M M, Ismail M. Review of the data-driven methods for electricity fraud detection in smart metering systems. Energies, 2023, 16(6): 2852-2853.

[17] MT Ibraheem Al-Naib A, Abdullah Hamad B. A Cost-Effective Method for Power Factor Metering Systems. International journal of electrical and computer engineering systems, 2022, 13(5): 409-415.

[18] Bayati N, Baghaee H R, Savaghebi M. EMD/HT-based local fault detection in DC microgrid clusters. IET Smart Grid, 2022, 5(3): 177-188.

[19] Cao W, Zhang F, Chen X. A Study on Fault Localization Method of Three-Terminal Multi-Section Overhead Line–Cable Hybrid Line Using MEEMD Combined with Teager Energy Operator Algorithm. Processes, 2024, 12(7): 1360-1362.

[20] Gheisari M, Hamidpour H, Liu Y, Saedi P, Raza A, Jalili A, Rokhsati H, Amin R. Data Mining Techniques for Web Mining: A Survey. Artificial Intelligence and Applications, 2023, 1(1): 3-10.